FBXW7 regulates endothelial barrier function by suppression of the cholesterol synthesis pathway and prenylation of RhoB

Manon C. A. Pronk[a], Jisca Majolée[a], Anke Loregger[b], Jan S. M. van Bezu[a], Noam Zelcer[b], Peter L. Hordijk[a], and Igor Kovačević[a,*]

[a]Department of Physiology, Amsterdam Cardiovascular Sciences, and [b]Department of Medical Biochemistry, Amsterdam University Medical Centers, 1081 HV Amsterdam, The Netherlands

ABSTRACT **Rho GTPases control both the actin cytoskeleton and adherens junction stability and are recognized as essential regulators of endothelial barrier function. They act as molecular switches and are primarily regulated by the exchange of GDP and GTP. However, posttranslational modifications such as phosphorylation, prenylation, and ubiquitination can additionally alter their localization, stability, and activity. F-box proteins are involved in the recognition of substrate proteins predestined for ubiquitination and subsequent degradation. Given the importance of ubiquitination, we studied the effect of the loss of 62 members of the F-box protein family on endothelial barrier function in human umbilical vein endothelial cells. Endothelial barrier function was quantified by electrical cell impedance sensing and macromolecule passage assay. Our RNA interference–based screen identified FBXW7 as a key regulator of endothelial barrier function. Mechanistically, loss of FBXW7 induced the accumulation of the RhoB GTPase in endothelial cells, resulting in their increased contractility and permeability. FBXW7 knockdown induced activation of the cholesterol biosynthesis pathway and changed the prenylation of RhoB. This effect was reversed by farnesyl transferase inhibitors and by the addition of geranylgeranyl pyrophosphate. In summary, this study identifies FBXW7 as a novel regulator of endothelial barrier function in vitro. Loss of FBXW7 indirectly modulates RhoB activity via alteration of the cholesterol biosynthesis pathway and, consequently, of the prenylation status and activity of RhoB, resulting in increased contractility and disruption of the endothelial barrier.**

Monitoring Editor
Mark H. Ginsberg
University of California, San Diego

Received: May 1, 2018
Revised: Dec 21, 2018
Accepted: Dec 27, 2018

INTRODUCTION

Endothelial cells (ECs) line all blood and lymph vessels throughout the body. They form a monolayer of tightly adherent cells that regulates the transmigration of leukocytes and transport of plasma proteins from the circulation into the tissues. Proper function of the endothelial barrier is crucial, as its dysfunction is a hallmark of chronic inflammatory diseases that can result in edema and tissue damage (Lee and Slutsky, 2010). Adherens junctions (AJs) serve as a bridge connecting the actin cytoskeleton of neighboring ECs (Dejana 1996) and are composed of multiple proteins, including the transmembrane protein vascular endothelial-cadherin (VE-cadherin)

This article was published online ahead of print in MBoC in Press (http://www.molbiolcell.org/cgi/doi/10.1091/mbc.E18-04-0259) on January 2, 2019.

No potential conflicts of interest were disclosed.

Author contributions: I.K., P.L.H., and N.Z. conceived the project and designed the experiments. M.C.A.P., J.M., A.L., and I.K. designed and performed the experiments and analyzed the data. J.S.M.v.B. performed the experiments. M.C.A.P., J.M., I.K., A.L., N.Z., and P.L.H. wrote the article.

*Address correspondence to: Igor Kovačević (i.kovacevic@vumc.nl).

Abbreviations used: AJ, adherens junction; ANOVA, analysis of variance; BSA, bovine serum albumin; EC, endothelial cell; ECIS, electrical cell–substrate impedance sensing; esiRNA, endoribonuclease-prepared small interfering RNA; esiEGFP, esiRNA targeting enhanced green fluorescent protein; FDR, false discovery rate; FPP, farnesyl pyrophosphate; FTI, farnesyl transferase inhibitor; GAP, GTPase-activating protein; GEF, guanine-nucleotide exchange factors; GGPP, geranylgeranyl pyrophosphate; GGTI, geranylgeranyl transferase inhibitor; HA, hemagglutinin; HRP, horseradish peroxidase; HSA, human serum albumin; HUVEC, human umbilical vein endothelial cell; LDLR, low-density lipoprotein receptor; PBS, phosphate-buffered saline; PFA, paraformaldehyde; shRNA, short hairpin RNA; siNT, nontargeting siRNA; siRNA, small interfering RNA; SQLE, squalene epoxidase; SREBP, sterol-regulatory element binding protein; VE-cadherin, vascular endothelial-cadherin.

and intracellular adaptor proteins such as α- and β-catenin, which link VE-cadherin to the actin cytoskeleton (Giannotta *et al.*, 2013). Importantly, the dynamics of the cytoskeleton, which allow force-generation parallel or perpendicular to cell–cell contacts, can stabilize or disrupt AJs (Hordijk *et al.*, 1999; Abu Taha and Schnittler, 2014).

Important regulators of AJs and of the actin cytoskeleton are the Rho GTPases. It is well established that Rac1 and Cdc42 promote endothelial barrier stability (Wojciak-Stothard and Ridley, 2002), while RhoA activation leads to endothelial barrier disruption (Van Nieuw Amerongen *et al.*, 2000). Activity of Rho GTPases is primarily regulated by a conformational change that is dependent on GDP or GTP binding (Cherfils and Zeghouf, 2013). The GTP-bound conformation enables interaction with downstream signaling proteins. Rho GTPases are activated by guanine-nucleotide exchange factors (GEFs), which promote the exchange of GDP for GTP, and by GTPase-activating proteins (GAPs), which stimulate the hydrolysis of GTP, leading to GTPase inactivation (Bos *et al.*, 2007). Inactive Rho GTPases are protected from ubiquitin-dependent degradation by binding to guanine-nucleotide dissociation inhibitor in the cytosol (Garcia-Mata *et al.*, 2011). It has become increasingly clear that nucleotide binding and the interaction with GEFs and GAPs is one of several mechanisms that regulate Rho GTPase activity, as Rho GTPases can also be phosphorylated, prenylated, and ubiquitinated to fine-tune their function (Schaefer *et al.*, 2014; Hodge and Ridley, 2016).

Among these posttranslational modifications, prenylation of Rho GTPases is a key determinant of their function. Prenylation targets Rho GTPases to the correct subcellular location and is important for interactions with regulatory proteins and downstream signaling effectors. RhoB is unique among the Rho GTPases, because it can be both geranylgeranylated and farnesylated (Adamson *et al.*, 1992). Farnesyl and geranylgeranyl are isoprenoids that are generated through the cholesterol synthesis pathway and covalently attached to the CAAX-box at the C-terminus of Rho GTPases through the activity of the enzymes farnesyl transferase and geranylgeranyl transferase I, respectively. The geranylgeranylated form of Rho GTPases is targeted for proteolysis (Von Zee and Stubbs, 2011) and is considered to be inactive, while the farnesylated form is active (Mazieres *et al.*, 2005). Accordingly, inhibition of farnesylation of RhoB was shown to reduce vascular cell proliferation, increase endothelium-dependent vasodilatation, and reduce vasoconstriction of pulmonary arteries in an animal model of hypoxia-induced pulmonary hypertension (Duluc *et al.*, 2017).

Besides prenylation, ubiquitination is an important posttranslational modification that regulates the protein stability of both RhoA and RhoB (Wei *et al.*, 2013; Kovačević *et al.*, 2018). During the ubiquitination process, the small protein ubiquitin (76 amino acids) is covalently attached to substrate proteins to selectively target them to the proteasome or to lysosomes for degradation. Ubiquitination consists of three steps whereby ubiquitin is activated by an E1 ubiquitin enzyme, transferred to an ubiquitin-conjugating enzyme E2, and attached to a substrate as monoubiquitin or a polyubiquitin by an E3 ligase (Pickart and Eddins, 2004). The E3 ligases are characterized by several defining motifs that allow direct or indirect ubiquitination of substrates (Ardley and Robinson, 2005). One family of E3 ligases, the Cullin RING (Really Interesting New Gene) ligases form large protein complexes; the SKP1-Cullin1-FBP ligase is a well-characterized example (Cardozo and Pagano, 2004). In this complex, Cullin-1 is the central adaptor protein that interacts via Rbx1 with the E2 ubiquitin ligase and with the F-box protein via Skp1. In this E3 ligase complex, the F-box protein acts as a specific recognition receptor that dictates the substrates for ubiquitination and subsequent degradation. The F-box family contains three groups of proteins, which are named according to their structure: the FBWs contain a WD-40 repeat; the FBLs contain a leucine-rich repeat; and the FBXs, which do not contain a WD-40 or leucine-rich repeat but often have other protein–protein interaction domains. A central question pertaining to F-box proteins is resolving the function of each individual F-box protein family member. The members that have been studied so far are mostly associated with the control of proliferation via the degradation of cyclins (Cardozo and Pagano, 2004). Owing to their structural diversity, F-box proteins can bind several different substrate proteins and are involved in the pathogenesis of various human diseases, including Parkinson's disease and cancer (Wang *et al.*, 2014; Zhou *et al.*, 2016). Besides the function of FBXW7 in angiogenesis and inflammation (Izumi *et al.*, 2012; Zhao *et al.*, 2013), the role of other F-box proteins in endothelium has not been studied in detail.

In the current study, we aimed to determine whether F-box proteins play a role in endothelial barrier function. Using primary human umbilical vein endothelial cells (HUVECs) in combination with endoribonuclease-prepared small interfering RNA (esiRNA)-mediated knockdown of F-box proteins, we found that FBXW7 is involved in regulation of the endothelial barrier. We further showed that cells lacking FBXW7 had a contractile phenotype that results in reduced barrier function and increased permeability both in resting and thrombin-stimulated cells. This phenotype can be attributed to the increased abundance of the contraction-inducing RhoB GTPase. Concomitantly, we found that FBXW7 depletion induced activation of the cholesterol synthesis pathway in ECs and thereby impaired both the prenylation and degradation of RhoB.

RESULTS

An esiRNA screen of F-box proteins identified both positive and negative regulators of endothelial barrier function

To identify new ubiquitination regulators that are important for endothelial barrier function, we screened a custom library of esiRNAs (Sigma) targeting 62 F-box proteins in primary HUVECs. The targets comprise members of all three different classes of F-box proteins (Table 1). Electrical cell–substrate impedance sensing (ECIS) was used to measure endothelial barrier function of HUVECs before, during, and after transfection with esiRNAs. The screen was repeated four times with four different pools of HUVECs, each derived from three different donors. The endothelial barrier function was measured in real time for 72 h after transfection and was then evaluated (Figure 1A). For data analysis, the mean delta increase in endothelial barrier resistance of each F-box protein esiRNA was compared with the mean delta increase of the control. The only significant hit in this screen after false discovery rate (FDR) correction was F-box/WD repeat-containing protein 7 (FBXW7) ($p = 0.0079$) (Figure 1B, depicted in red). Other proteins that showed a significant effect before FDR correction were FBXL19, FBXL17, FBXL16, FBXO18, and FBXO28. However, some of the tested F-box proteins showed large intraexperimental variation, which could have influenced the interpretation of the results. Most of the tested F-box protein esiRNA did not show large effects compared with the esiRNA targeting enhanced green fluorescent protein (esiEGFP) control. This might be due to redundancy between F-box proteins or their irrelevance for regulation of endothelial barrier function. While loss of FBXW7 showed the largest decrease in barrier function, depletion of FBXL19 induced the largest increase in barrier function (Figure 1C). The effects of FBXW7 and FBXL19 esiRNAs were corroborated by lentivirally expressed short hairpin RNA (shRNA) targeting the same proteins (Supplemental Figure 1). These findings indicate that a limited subset of F-box proteins is involved

FBXL	FBXO		FBXW
SKP2	CCNF	FBXO27	BTRC
FBXL2	FBXO2	FBXO28	FBXW2
FBXL3	FBXO3	FBXO30	FBXW4
FBXL4	FBXO4	FBXO32	FBXW5
FBXL5	FBXO5	FBXO33	FBXW7
FBXL6	FBXO6	FBXO34	FBXW8
FBXL7	FBXO7	FBXO36	FBXW10
FBXL10	FBXO8	FBXO38	AC005838.2
KDM2A	FBXO9	FBXO39	FBXW11
FBXL12	FBXO10	FBXO41	
FBXL13	FBXO11	FBXO42	
FBXL14	FBXO15	FBXO43	
FBXL16	FBXO16	FBXO44	
FBXL17	FBXO17	FBXO45	
FBXL18	FBXO18	FBXO46	
FBXL19	LMO7		
FBXL20	FBXO21		
FBXL21	FBXO22		
FBXL22	FBXO24		

esiRNAs targeting 19 FBXL, 34 FBXO and 9 FBXW proteins were included in the screen.

TABLE 1: F-box proteins included in the screen, with esiRNA targeted F-box proteins grouped into three protein families: F-box and leucine-rich repeat (FBXL), F-box only (FBXO), and F-box and WD40 domain (FBXW).

in the regulation of the endothelial barrier and that FBXW7 is a positive regulator of endothelial barrier function.

FBXW7 knockdown impairs endothelial barrier function

To expand the results from the esiRNA screen, we repeated the experiments with independent siRNAs (ON-TARGET plus SMART pools) in different pools of primary HUVECs. As control in these experiments, cells were transfected with nontargeting siRNA (siNT). First, we confirmed that FBXW7 mRNA was effectively down-regulated in cells that were transfected with FBXW7 siRNA. Figure 2A shows that there is ~95% loss of FBXW7 mRNA in FBXW7 knockdown cells. siRNA-mediated loss of FBXW7 in ECs resulted in a significantly decreased barrier resistance compared with control cells (Figure 2, B and C). Resolving the endothelial resistance measurements into separate components reflecting cell–cell and cell–matrix interaction (Moy *et al.*, 2000) showed that loss of FBXW7 did not significantly change cell–matrix interaction compared with control cells (Figure 2, D and E). However, the cell–cell interaction was significantly lower in FBXW7 knockdown cells compared with control cells (Figure 2, F and G). Because the endothelial resistance measurements showed significant effects on cell–cell interaction, we next focused on the morphology of the actin cytoskeleton and AJs in FBXW7 knockdown cells. Phalloidin staining showed more intense overall F-actin staining and formation of contractile actin rings in FBXW7 knockdown cells (Figure 2H). Furthermore, immunostaining of the cell–cell adhesion protein VE-cadherin revealed discontinuous VE-cadherin distribution in FBXW7-depleted cells (Figure 2H). These findings were confirmed by use of an shRNA targeting FBXW7 (Supplemental Figure 2). Furthermore, we analyzed the colocalization of VE-cadherin and F-actin. This analysis showed that colocalization of VE-cadherin and F-actin is significantly lower in FBXW7 knockdown cells compared with control cells (Figure 2, I and J). Finally, FBXW7 knockdown did not significantly reduce the number of ECs at 72 h posttransfection (Figure 2K). Together, these findings suggest that decreased barrier function in FBXW7 knockdown cells is induced by increased stress fiber formation and loss of stable, junctional VE-cadherin distribution.

Loss of FBXW7 delays recovery from thrombin-induced loss of barrier integrity

In the human circulation, the endothelium can become exposed to many vasoactive agents. Here, we studied the effect of the proinflammatory protease thrombin on endothelial barrier function in control and FBXW7 knockdown cells. The ability of the cells to recover their barrier function after thrombin stimulation is another parameter that gives information about endothelial junction dynamics. Stimulation with thrombin (1 U/ml) resulted in a rapid drop in endothelial barrier resistance (Figure 3A). This drop in resistance was not significantly different between control and FBXW7 knockdown cells (Figure 3B). In contrast, the recovery after thrombin stimulation at 3 h poststimulation was significantly reduced in FBXW7 knockdown cells (Figure 3C).

To test the effect of thrombin on the endothelial barrier in an independent assay, we measured macromolecule passage across endothelial monolayers stimulated with thrombin. In line with the ECIS results, the FBXW7 knockdown cells displayed increased horseradish peroxidase (HRP) leakage compared with control cells under basal conditions (Figure 3D). Stimulation with thrombin increased overall permeability of the monolayer, which was enhanced in cells lacking FBXW7. The permeability of FBXW7 knockdown cells was higher compared with the control cells at all time points, with statistically significant difference at 1.5 and 2 h after thrombin stimulation (Figure 3D).

To analyze whether the effect on permeability correlated with changes in cell morphology, we visualized F-actin and VE-cadherin in control and FBXW7 siRNA transfected cells. At 15 min after thrombin addition, we observed gaps and stress fiber formation in monolayers of both control and FBXW7 knockdown cells. However, the gaps appeared larger and the intensity of the F-actin contractile ring was higher in FBXW7 knockdown cells compared with control cells (Figure 3, E and I). Both FBXW7 knockdown and control cells displayed discontinuous and jagged VE-cadherin staining (Figure 3E) without significant difference in overall VE-cadherin levels (Figure 3G). At 3 h after thrombin treatment, we observed that control cells, although they still contained stress fibers, did not show interendothelial gaps anymore and that VE-cadherin distribution was more continuous and concentrated (Figure 3F). In contrast, gaps were still present in the monolayer of FBXW7 knockdown cells (Figure 3J). Additionally, at 3 h after thrombin treatment, FBXW7 knockdown cells showed less intense and discontinuous VE-cadherin staining compared with the control cells (Figure 3, F and H). In summary, FBXW7 knockdown cells recover at a slower rate after thrombin stimulation, possibly due to increased stress fiber formation and VE-cadherin turnover.

FBXW7 depletion increases RhoB levels

The increased formation of F-actin stress fibers that we observed in FBXW7 knockdown cells could be caused by increased expression and/or activity of Rho GTPases. Previously, RhoA was shown to be an important regulator of contraction induced by thrombin

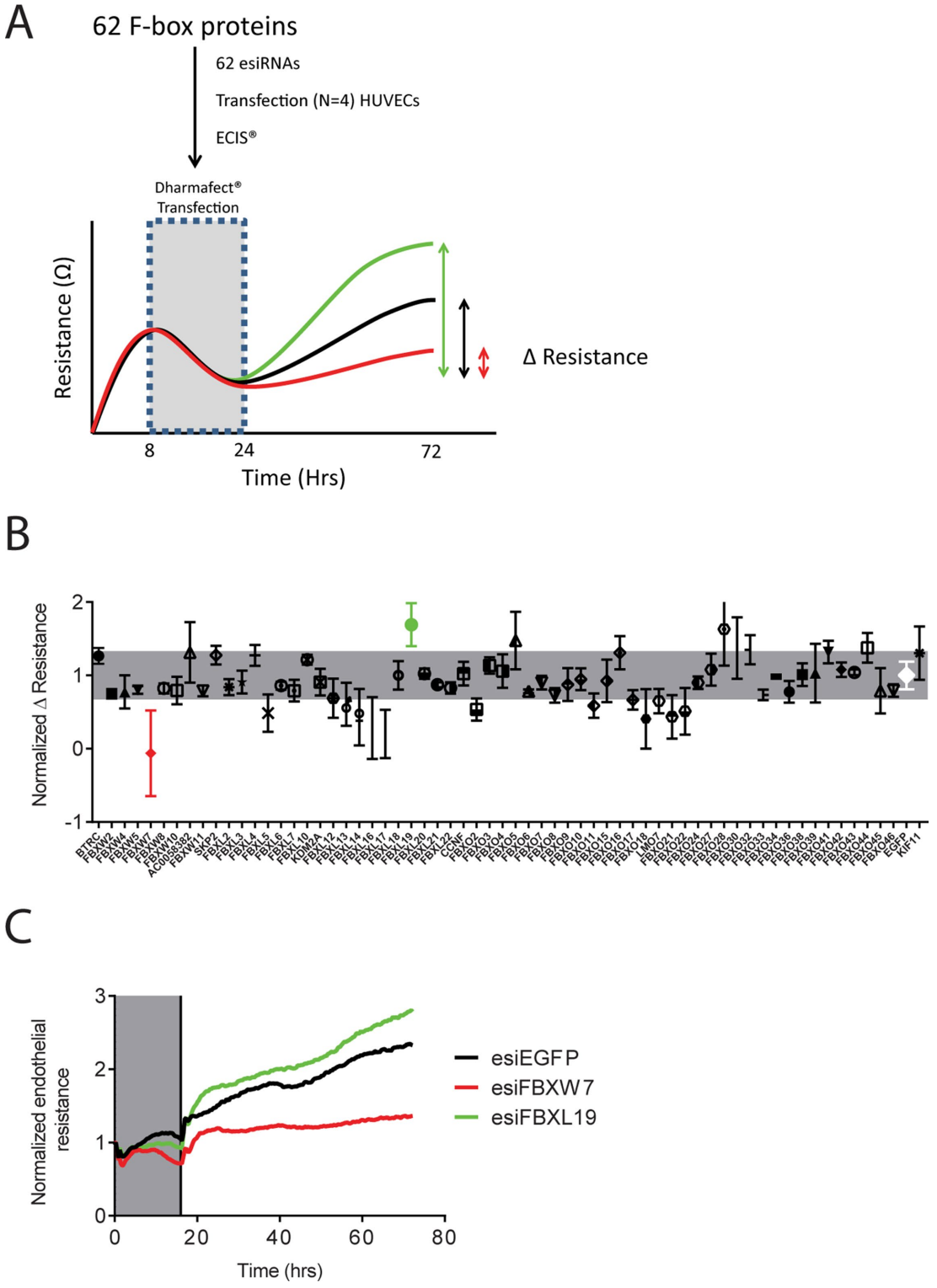

FIGURE 1: An esiRNA screen identifies F-box proteins involved in endothelial barrier function. (A) Schematic representation of the esiRNA screen. Sixty-two esiRNAs were transfected into pools of HUVECs seeded on 96W10idf ECIS arrays ($n = 4$). Endothelial resistance was measured for 72 h following transfection. A schematic ECIS graph is shown: green, an example of the enhancement of the endothelial barrier after knockdown; red, an example of disruption of the endothelial barrier after knockdown; black, a control EGFP esiRNA. (B) Overview of the mean delta of electrical resistance from the start of transfection until the 72 h time point for each esiRNA. White, the EGFP control; green, the highest value; red, the lowest value. The gray bar represents the threshold value at ±33% of the EGFP control. Data points represent mean ± SEM ($n = 4$). (C) Effect of loss of FBXL19, EGFP, and FBXW7 on basal endothelial barrier function. Data represent normalized average values from the start of transfection ($t = 0$) until the end of $n = 4$ experiments.

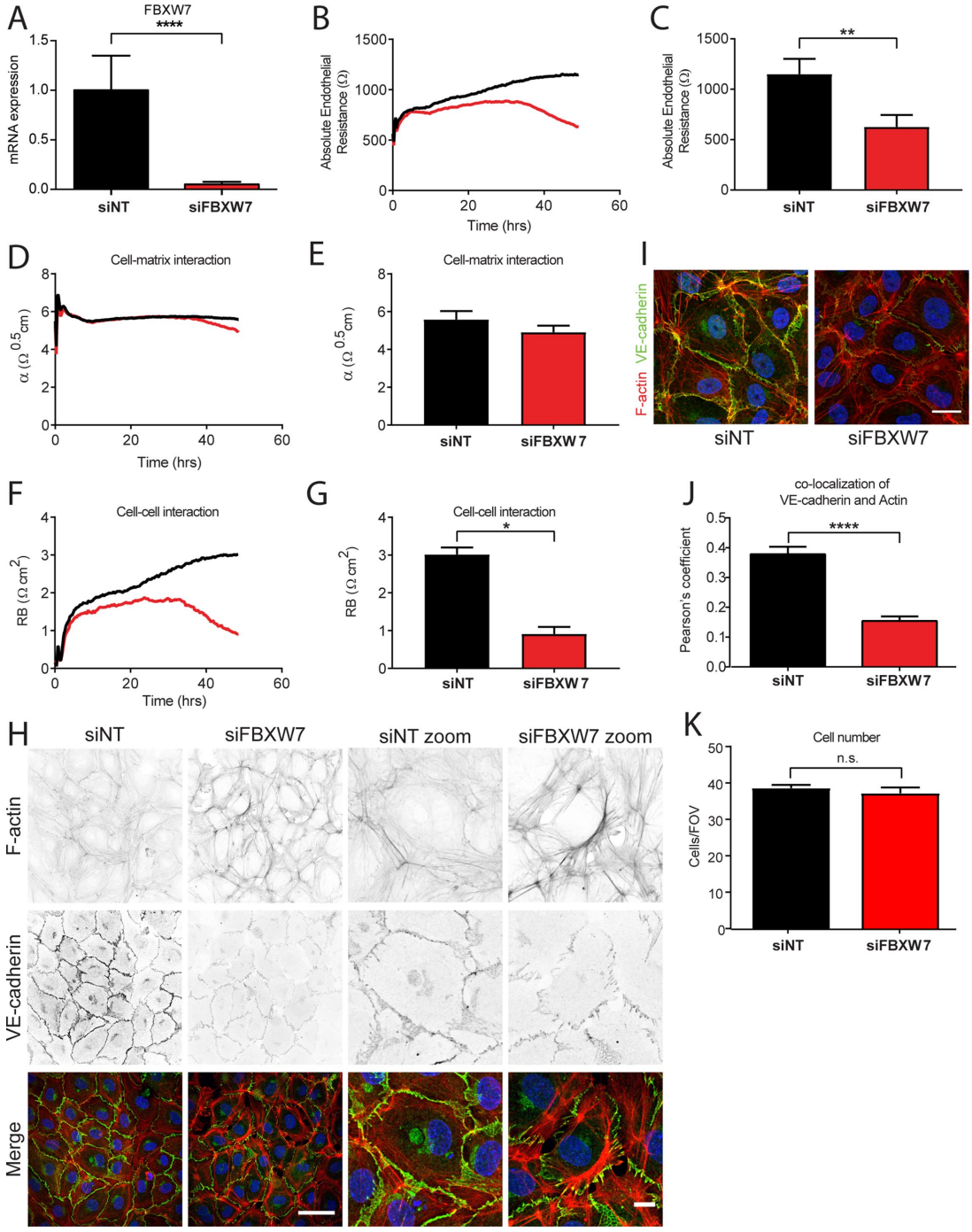

FIGURE 2: FBXW7 knockdown causes decreased endothelial barrier function by increased contractile ring formation. (A) HUVECs were transfected with siNT and siFBXW7 and cultured for 72 h. Total RNA was isolated, and expression of the indicated genes was determined by quantitative PCR. Each bar and error bar represent the mean ± SD ($n = 3$); ****, $p < 0.0001$. (B) Effect of the loss of FBXW7 on basal endothelial barrier function. (C) Basal endothelial barrier function at $t = 72$ h. (D) Absolute endothelial resistance attributable to cell–matrix adhesion (α) of control and FBXW7 knockdown cells. (E) α at $t = 72$ h. (F) Absolute endothelial resistance attributable to cell–cell adhesion (Rb) of control and FBXW7 knockdown cells. (G) Rb at $t = 72$ h. (H) Immunofluorescence staining of VE-cadherin (green), F-actin (red), and nuclei (blue) in HUVECs for visualization of AJs and actin fibers following loss of FBXW7. Scale bars: 50 μm; scale bar in the zoomed images: 10 μm. Representative images of three experiments. (I) Immunofluorescence staining of VE-cadherin (green), F-actin (red), and nuclei (blue) in HUVECs for visualization of colocalization of AJs and actin fibers following loss of FBXW7. Scale bar: 20 μm. (J) Quantification of Mander's coefficient of colocalization of VE-cadherin with actin from I was performed using ImageJ and JACoP plug-in (Bolte and Cordelieres, 2006) ($n = 12$). (K) Cell number quantification in control and FBXW7 knockdown cells at $t = 72$ h. DAPI-stained nuclei were counted per field of view ($n = 12$). ECIS data represent average values (line graphs, representing barrier formation, Rb or α from medium change at 16 h after transfection [$t = 0$] until the end of the experiment) or mean ± SEM (bar graphs) of $n = 3$ experiments. *, $p < 0.05$; **, $p < 0.01$, paired t test. Colocalization data represent mean ± SEM of $n = 3$ experiments. ****, $p < 0.0001$, unpaired t test. siNT, nontargeting siRNA.

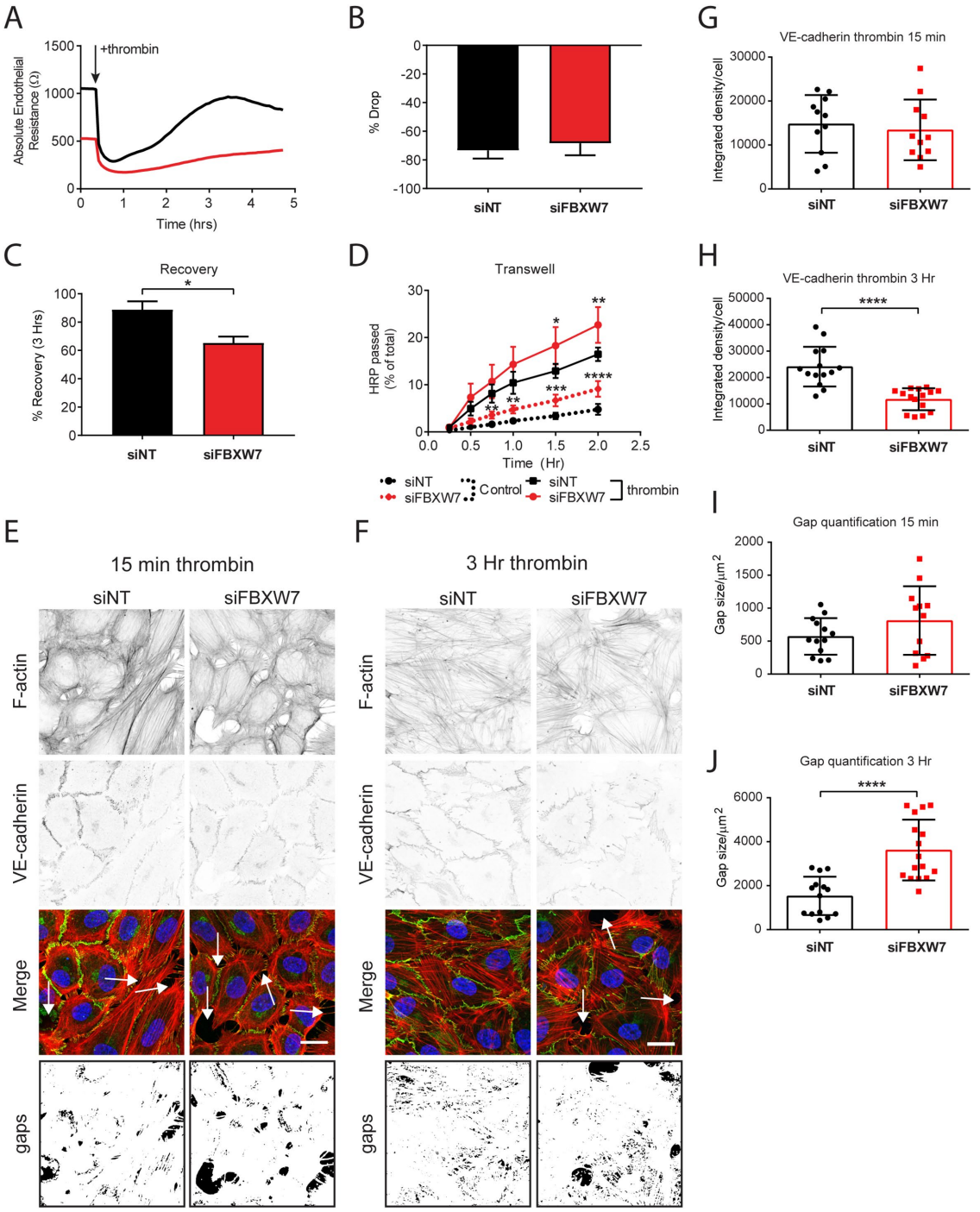

FIGURE 3: The effect of thrombin-induced hyperpermeability on FBXW7 knockdown cells. (A) Thrombin-induced endothelial barrier disruption in FBXW7 knockdown cells. Arrow indicates addition of thrombin (1U/ml). (B) The thrombin response (% decrease in normalized resistance) in control vs. FBXW7 knockdown cells. Values represent the percentage drop at the lowest point of resistance following the addition of thrombin. (C) The percent recovery at 3 h after thrombin relative to the respective start values in control vs. FBXW7 knockdown cells. (D) Time-dependent effects of control and FBXW7 knockdown on the passage of HRP across control and thrombin-stimulated HUVECs. Data represent average of three experiments. (E,F) Immunofluorescence staining of VE-cadherin (green), F-actin (red), and nuclei (blue) in HUVECs for visualization of AJs and actin fibers following loss of FBXW7 and after 15 min (E) and 3 h (F) of thrombin stimulation. Arrows indicate gaps. Scale bars: 20 μm. Images are representative of three experiments. (G,H) Quantification of VE-cadherin staining intensity at 15 min (G) and 3 h (H) after thrombin stimulation. Integrated density of VE-cadherin staining per cell was calculated using ImageJ software. $n = 12$. (I, J) Quantification of interendothelial gap size at 15 min (I) and 3 h (J) after thrombin stimulation. Gap size was measured using ImageJ software. ECIS data represent average values or mean ± SEM (bar graphs) of $n = 3$ experiments. *, $p < 0.05$, paired t test. D shows average values of three experiments performed in triplicate. *, $p < 0.05$; **, $p < 0.01$; ***, $p < 0.001$; ****, $p < 0.0001$, in Dunnett's post hoc analysis of two-way ANOVA multiple-comparisons test. siNT, nontargeting siRNA.

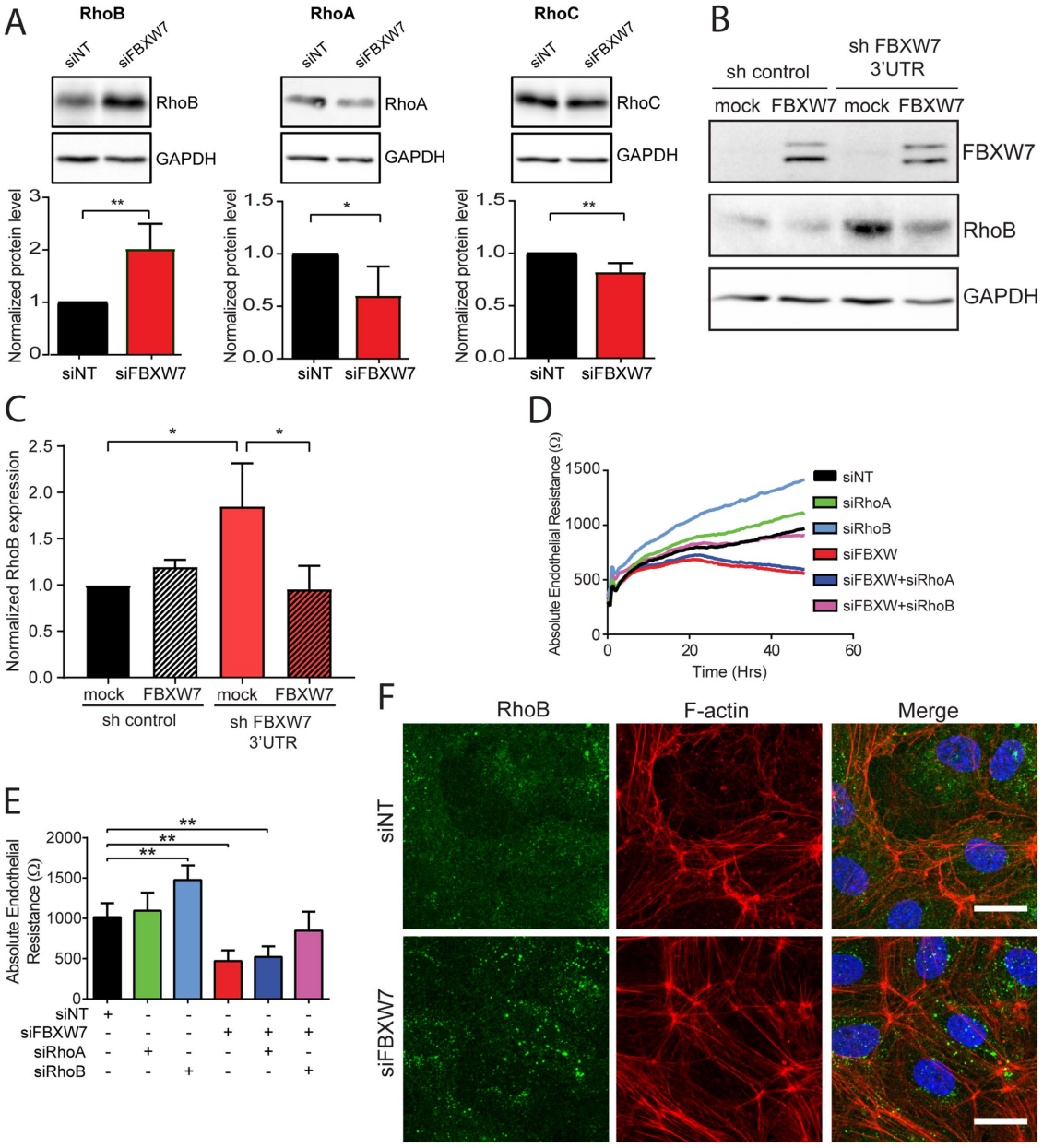

FIGURE 4: FBXW7 knockdown increased RhoB levels in HUVECs. (A) Western blot of whole-cell lysates showing the effect of FBXW7 knockdown on expression of RhoB, RhoA, and RhoC in HUVECs. Representative blots from four experiments are shown. GAPDH is included as a loading control. Bar graph represents mean ± SD of RhoB expression from four individual experiments, all relative to GAPDH and normalized to siNT. (B) Western blot of the FBXW7 rescue experiment. Cells were infected with control shRNA lentivirus (sh control) or lentivirus carrying shRNA that targets the 3′UTR of FBXW7 mRNA in combination with lentivirus carrying empty pTRIPZ doxocycline-inducible vector or pTRIPZ vector containing FBXW7 cDNA. Doxocycline was added 24 h before cell lysis. GAPDH is shown as loading control. (C) Quantification of the RhoB levels from B. Bar graphs represent mean ± SD of RhoB expression from three individual experiments, all relative to GAPDH and normalized to sh control + mock condition. (D, E) Effect of loss of RhoA and RhoB in combination with FBXW7 knockdown on basal endothelial barrier function. (E) Quantification of basal endothelial barrier function at $t = 72$ h. (F) Immunofluorescence staining of RhoB (green), F-actin (red), and nuclei (blue) in control and FBXW7 knockdown HUVECs. Scale bar: 20 μm. Images are representative of three experiments. ECIS data represent average values (line graphs, representing barrier formation from medium change at 16 h after transfection [$t = 0$] until the end of the experiment) or mean ± SEM (bar graphs) of $n = 4$ experiments. *, $p < 0.05$, paired t test. **, $p < 0.01$, Dunnett's post hoc analysis of one-way ANOVA.

stimulation (Van Nieuw Amerongen *et al.*, 2000). We recently showed that, besides RhoA, RhoB mediates the contraction of ECs (Pronk *et al.*, 2017), and we therefore analyzed RhoB protein abundance. We found that FBXW7 knockdown cells showed a markedly increased level of RhoB compared with control cells (Figure 4A). In contrast, RhoA and to lesser extent RhoC levels were reduced upon FBXW7 depletion (Figure 4A). To exclude the possibility that the effects we observed on RhoB levels in FBXW7 knockdown cells were

unspecific, we performed a rescue experiment. In this experiment, we depleted FBXW7 by using lentiviruses encoding an shRNA that targets the 3'UTR of the FBXW7 mRNA. In accordance with the siRNA experiments, we found that shFBXW7 also increases RhoB expression in these experiments (Figure 4B). Ectopic re-expression of FBXW7 from a doxocycline-inducible lentiviral vector reduced the expression of RhoB to the levels found in control cells. To test whether the increase in RhoB in FBXW7 knockdown cells was the main cause of the decreased barrier function, we performed knockdown of FBXW7 in combination with loss of RhoA or of RhoB. We found that loss of RhoB significantly increased endothelial barrier resistance, while RhoA knockdown did not demonstrate differences compared with control cells (Figure 4, C and D). Depletion of FBXW7 decreased endothelial barrier significantly compared with control cells, which is in line with the data in Figure 2. Combined knockdown of FBXW7 and RhoA induced a decrease in endothelial barrier resistance similar to the single FBXW7 knockdown. On the other hand, endothelial resistance measured in cells with double knockdown of FBXW7 and RhoB was not significantly different compared with control cells (Figure 4, C and D). In additional experiments, we tested whether single siRNA sequences targeting FBXW7 similarly enhanced RhoB expression and disrupted endothelial barrier function, as we observed with siRNA pool. We found that two out of four tested clones indeed increased the levels of RhoB, and this was accompanied by a significant loss of endothelial barrier integrity (Supplemental Figure 3, A and B). Because subcellular targeting of Rho GTPases is important for their function, we analyzed RhoB localization in control and FBXW7 knockdown cells by confocal microscopy. In line with immunoblotting, immunostaining for RhoB showed that FBXW7 knockdown cells contained more RhoB localized to vesicles compared with control cells (Figure 4E). In summary, our results indicate that the decrease of endothelial barrier integrity induced by the loss of FBXW7 expression is to a large extent the result of increased levels of RhoB protein.

Loss of FBXW7 activates the cholesterol synthesis pathway in ECs

In previous studies, FBXW7 was shown to regulate ubiquitination and abundance of RhoA in gastric cancer (Li *et al.*, 2016). We recently found that another CRL complex, namely, Cullin-3/KCTD10, is responsible for RhoB ubiquitination in ECs (Kovačević *et al.*, 2018). We tested whether ubiquitination of RhoB is also regulated by FBXW7. Using an in vivo ubiquitination assay in HEK293T cells, we did not observe an increase in RhoB ubiquitination upon coexpression of FBXW7 (Supplemental Figure 4A). In accordance with this, we also did not observe reduced ubiquitination of endogenous RhoB in FBXW7-depleted ECs (Supplemental Figure 4B).

FBXW7 has previously been demonstrated to control the cholesterol biosynthesis pathway in hepatocytes owing to its ability to regulate the level of the sterol-regulatory element binding protein (SREBP) transcription factors (Sundqvist *et al.*, 2005; Loregger *et al.*, 2017). To test whether this is also the case in ECs, we measured mRNA levels of several proteins that are part of the cholesterol pathway. In line with FBXW7 having a similar effect in ECs, its loss leads to increased expression of the SREBP-regulated target genes 3-hydroxy-3-methyl-glutaryl-coenzyme A reductase (*HMGCR*), squalene synthase (*SQS*), squalene epoxidase (*SQLE*), and the low-density lipoprotein receptor (*LDLR*) (Figure 5, A–D). For two of these genes, we tested whether increased mRNA expression also resulted in increased abundance of the encoded protein. We found that, mirroring the effects on mRNA levels, the protein abundance of SQLE was increased 2.5-fold in FBXW7 knockdown cells compared with control cells. Similarly, LDLR levels were increased twofold in FBXW7 knockdown cells compared with control cells (Figure 5E). These data

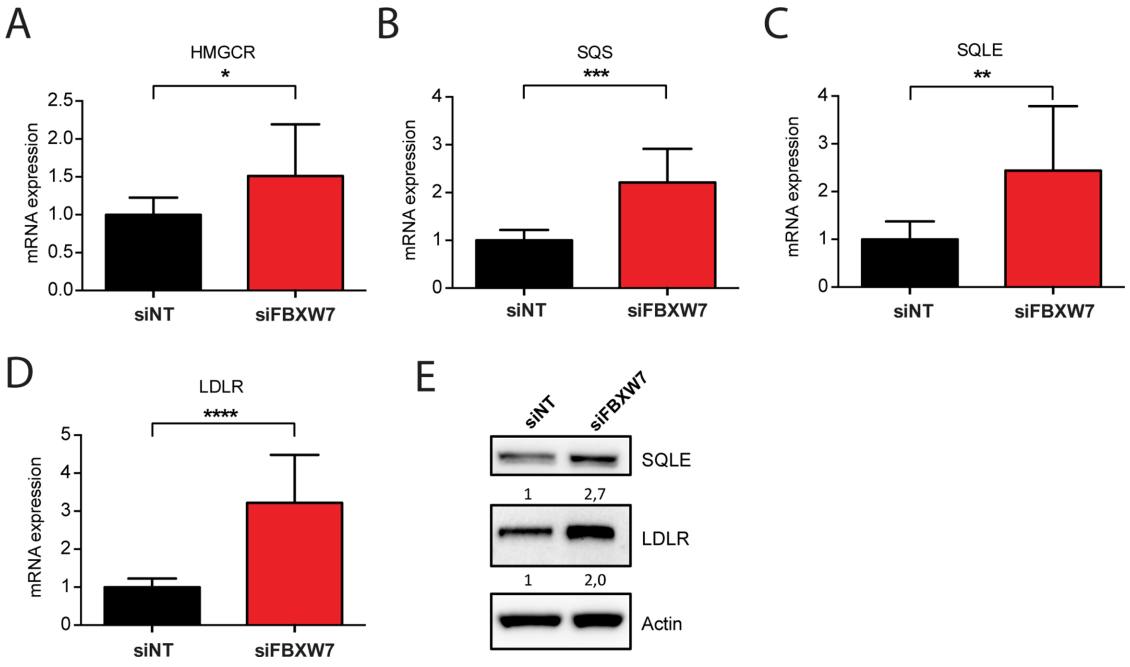

FIGURE 5: FBXW7 knockdown induces activation of the cholesterol synthesis pathway. (A–D) HUVECs were transfected with siNT and siFBXW7 and cultured for 72 h. Total RNA was isolated, and expression of the indicated genes was determined by quantitative PCR. Each bar and error bar represent the mean ± SD ($n = 3$); *, $p < 0.05$; **, $p < 0.01$; ***, $p < 0.001$; ****, $p < 0.0001$. (E) Western blot of whole-cell lysates showing the effect of FBXW7 knockdown on expression of SQLE and LDLR in HUVECs. Representative blots from four experiments are shown. Actin is included as a loading control. Numbers represent mean from four individual experiments all normalized to siNT.

are in line with a previous publication, in which FBXW7 knockdown was shown to lead to the activation of SREBPs in U2OS and HCT116 epithelial cancer cells (Sundqvist *et al.*, 2005) and activation of the cholesterol synthesis pathway. Together, these findings indicate that FBXW7 knockdown leads to the up-regulation of several components of the cholesterol synthesis pathway in ECs.

Stimulation of geranylgeranylation rescues disruption of endothelial barrier in FBXW7 knockdown cells

RhoB in ECs is mostly localized in vesicles; however, inhibition of RhoB ubiquitination redistributes RhoB predominantly to the plasma membrane (Kovačević *et al.*, 2018). In Figure 4B, we demonstrate that, in FBXW7 knockdown cells, the level of RhoB was increased, with the protein localizing both to and outside the vesicles. This finding, in combination with the up-regulation of the cholesterol pathway, led us to hypothesize that prenylation might play a role in redistribution of RhoB upon FBXW7 knockdown. Previously, it was shown that the cholesterol synthesis pathway and prenylation of RhoB are crucial for the regulation of RhoB levels (Stamatakis *et al.*, 2002). RhoB can be either farnesylated by farnesyl transferase or geranylgeranylated by geranylgeranyl transferase. Therefore, we treated control and FBXW7 knockdown cells for 24 h with a farnesyl transferase inhibitor (FTI), a geranylgeranyl transferase inhibitor (GGTI), or a combination of both at 48 h after transfection. In control cells, we observed no differences in endothelial resistance following treatment with FTI. Although the addition of GGTI alone or in combination with FTI induced an initial drop in electrical resistance, there were no statistically significant differences at 24 h after addition (Figure 6, A and B). As expected, FBXW7 knockdown cells without stimulation showed a drop in resistance in the 24 h during which they were monitored (Figure 6, C and D). When FTI was added to the FBXW7 knockdown cells, this drop was largely reversed, while no differences were seen with addition of GGTI alone or GGTI in combination with FTI compared with untreated FBXW7 knockdown cells (Figure 6, C and D).

In subsequent experiments, we analyzed the effects of FTI and GGTI on RhoB protein levels. In untreated FBXW7 knockdown cells, we found increased levels of RhoB. Treatment with FTI slightly increased RhoB levels in control cells but did not further increase RhoB in FBXW7 knockdown cells. Addition of GGTI to control cells, as well as combined treatment with FTI and GGTI, induced a more robust increase in RhoB protein levels compared with FTI treatment (Figure 6E).

Because prenylation is important for the localization of RhoB (Von Zee and Stubbs, 2011), we analyzed RhoB by immunofluorescence after addition of the inhibitors. FBXW7 knockdown cells resulted in more RhoB protein, stress fiber formation, and decreased VE-cadherin expression at the cell–cell contacts (Figure 6F; see also Figure 2). Treatment with FTI partially reduced stress fiber formation and restored the VE-cadherin distribution in FBXW7 knockdown cells (Figure 6F). Treatment with GGTI and the combined treatment of FTI and GGTI resulted in increased, homogeneously distributed RhoB throughout the cell in both control and FBXW7 knockdown cells. In the FBXW7 knockdown cells, we observed decreased VE-cadherin intensity compared with control cells (Figure 6F). Because addition of FTI protected against the barrier-disrupting effect of the loss of FBXW7, possibly by induction of geranylgeranylation of RhoB, we hypothesized that addition of geranylgeranyl pyrophosphate (GGPP) might also restore the disruptive effect of FBXW7 knockdown. Indeed, addition of GGPP resulted in the restoration of barrier function in FBXW7 knockdown cells to control cell levels, while addition of farnesyl pyrophosphate (FPP) did not show any significant effects (Figure 6G). Together, these data suggest that, due to the increased generation of isoprenoids originating from the cholesterol synthesis pathway, which is induced upon FBXW7 knockdown, RhoB is increasingly farnesylated, resulting in the accumulation of (active) RhoB in ECs.

RhoB prenylation is impaired in FBXW7 knockdown cells

Changes in protein prenylation can be assessed by analyzing the lipophilic properties of the protein using Triton X-114 extraction. This method was recently applied to study prenylation of Rab7 in neurons (Mohamed *et al.*, 2018). First, we tested whether distribution of RhoB between detergent-rich lipophilic and aqueous hydrophilic fractions is changed upon application of GGTI or FTI. We found that, in unstimulated cells, RhoB is predominantly detected in the detergent-rich lipophilic fraction (Figure 7A). Treatment of ECs with GGTI resulted in a complete shift of RhoB toward the aqueous fraction. In contrast, FTI did not change the distribution of RhoB between the aqueous and detergent-rich fractions. We then analyzed the distribution of RhoB in FBXW7 knockdown cells and found that the fraction of RhoB in the aqueous fraction was increased twofold when compared with control cells (Figure 7, B and C). Increased RhoB in this fraction in FBXW7 knockdown cells partially mimics geranylgeranyl transferase inhibition. In contrast, RhoB, RhoA, and RhoC are detected predominantly in the aqueous fraction and their lipophilic properties were not affected by FBXW7 knockdown.

In summary, our data suggest a novel model of the regulation of endothelial barrier function by FBXW7 (Figure 8). Knockdown of FBXW7 leads to increased activation of the cholesterol synthesis pathway, likely a result of SREBP stabilization (Sundqvist *et al.*, 2005). In this setting, more GGPP and FPP are available for prenylation, and as a consequence, RhoB is both more geranylgeranylated and farnesylated. Because farnesylated RhoB is protected from degradation (Duluc *et al.*, 2017), the amount of active RhoB increases, leading to increased stress fiber formation and barrier disruption. FTI can counteract this effect by switching the equilibrium toward geranylgeranylation of RhoB, which drives inactive RhoB to vesicles. Addition of GGPP rescues the siFBXW7-phenotype by promoting geranylgeranylation of RhoB (Figure 8).

DISCUSSION

We report here the results of an ECIS-based screen of esiRNA-mediated depletion of 62 F-box proteins in HUVECs. Our data show that, in this protein family, FBXW7 is a key positive regulator of endothelial barrier function. Knockdown of FBXW7 in resting ECs induces stress fiber formation and contractile actin ring formation, causing decreased barrier function both in resting and thrombin-stimulated cells. Depletion of FBXW7 also leads to up-regulation of RhoB protein levels and activation of the cholesterol synthesis pathway. The latter pathway is the source of isoprenoids, which are crucial modifiers of RhoB localization, activity, and stability (Adamson *et al.*, 1992; Von Zee and Stubbs 2011). These findings suggest that RhoB prenylation might be affected in FBXW7 knockdown cells, which could result in increased activity of RhoB and subsequent disruption of the endothelial barrier.

In parallel, we found that RhoA and RhoC levels were decreased in FBXW7 knockdown cells. This might be caused by the regulatory interactions that exist between RhoA, RhoB, and RhoC, affecting their respective expression levels (Pronk *et al.*, 2017). An siRNA-based F-box protein screen was previously performed to assess their effect on virus replication (Kainulainen *et al.*, 2016) and cell proliferation in several types of cancers (Machida and Dutta, 2007;

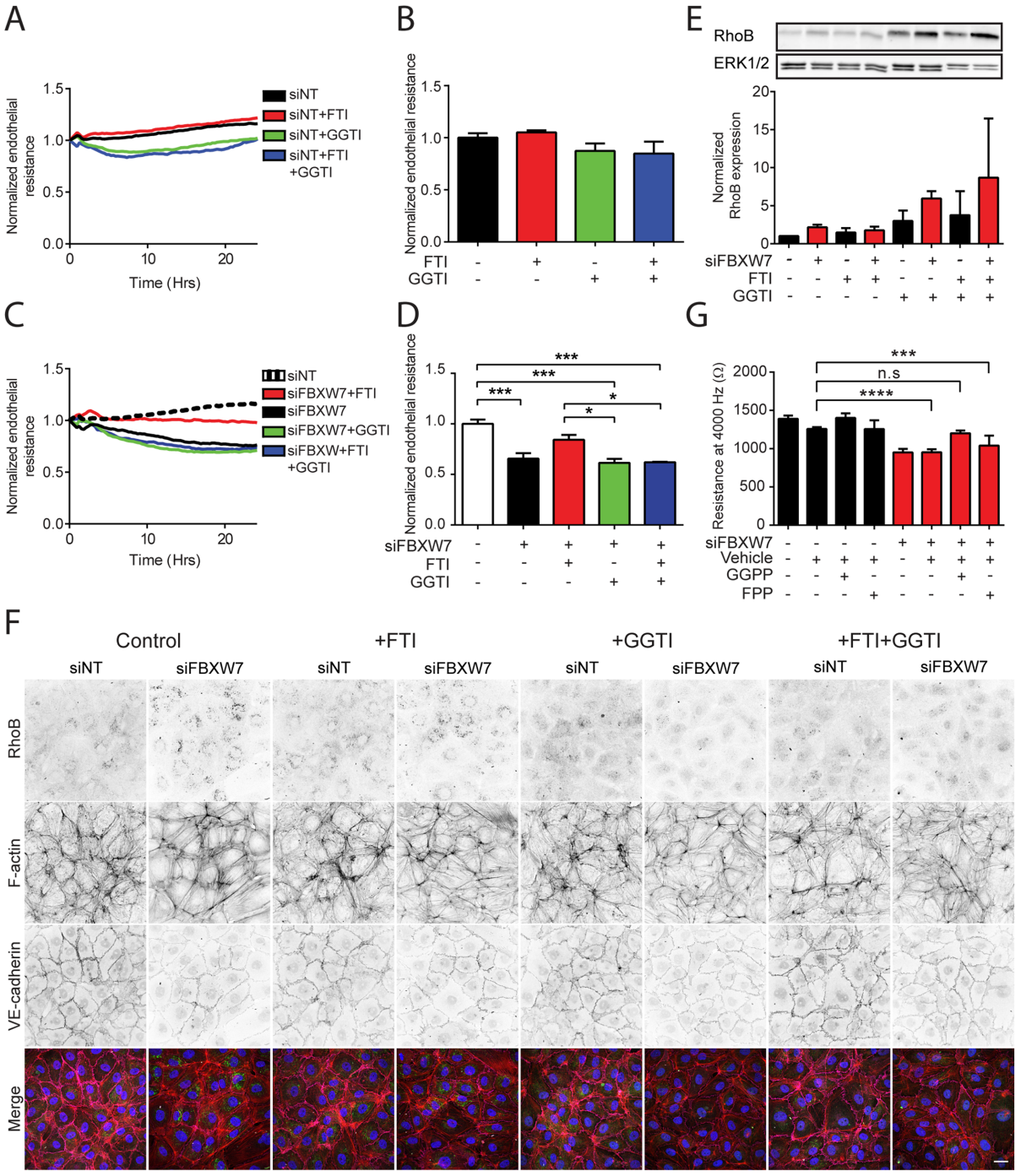

FIGURE 6: Endothelial barrier disruption is caused by impaired prenylation of RhoB in FBXW7 knockdown cells. (A) Effect of FTI (10 μm; red), GGTI (10 μm; green), and FTI + GGTI combination (blue) on normalized barrier function of control cells. $t = 0$ corresponds to 48 h after transfection. (B) Endothelial barrier function after 24 h stimulation with FTI + GGTI. (C) Effect of addition of FTI (red), GGTI (green), and FTI + GGTI combination (blue) on normalized barrier function of FBXW7 (black) knockdown and control (dashed) cells. $t = 0$ is 48 h after transfection. (D) Endothelial barrier function after 24 h stimulation with FTI + GGTI. (E) Western blot of whole-cell lysates showing the effect of FBXW7 knockdown and stimulation with FTI and GGTI on expression of RhoB in HUVECs. Representative blots from two experiments are shown. ERK1/2 is included as a loading control. Bar graph represents mean ± SD from two individual experiments all normalized to siNT. (F) Immunofluorescence staining of RhoB (green), F-actin (red), VE-cadherin (magenta), and nuclei (blue) in control and FBXW7 knockdown HUVECs stimulated with FTI, GGTI, or FTI + GGTI. Scale bar: 25 μm. Images are representative of three individual experiments. (G) Effect of GGPP (10 μm) and FPP (10 μm) on barrier function of control and FBXW7 knockdown cells. Data represent mean ± SD of $n = 2$ experiments performed in triplicate. In A–D data represent average values (line graphs, representing barrier function from addition of inhibitor 48 h after transfection [$t = 0$] until the end of the experiment) or mean ± SEM of $n = 3$ experiments performed in duplicate. *, $p < 0.05$; ***, $p < 0.001$; ****, $p < 0.0001$, Dunnett's post hoc analysis of one-way ANOVA.

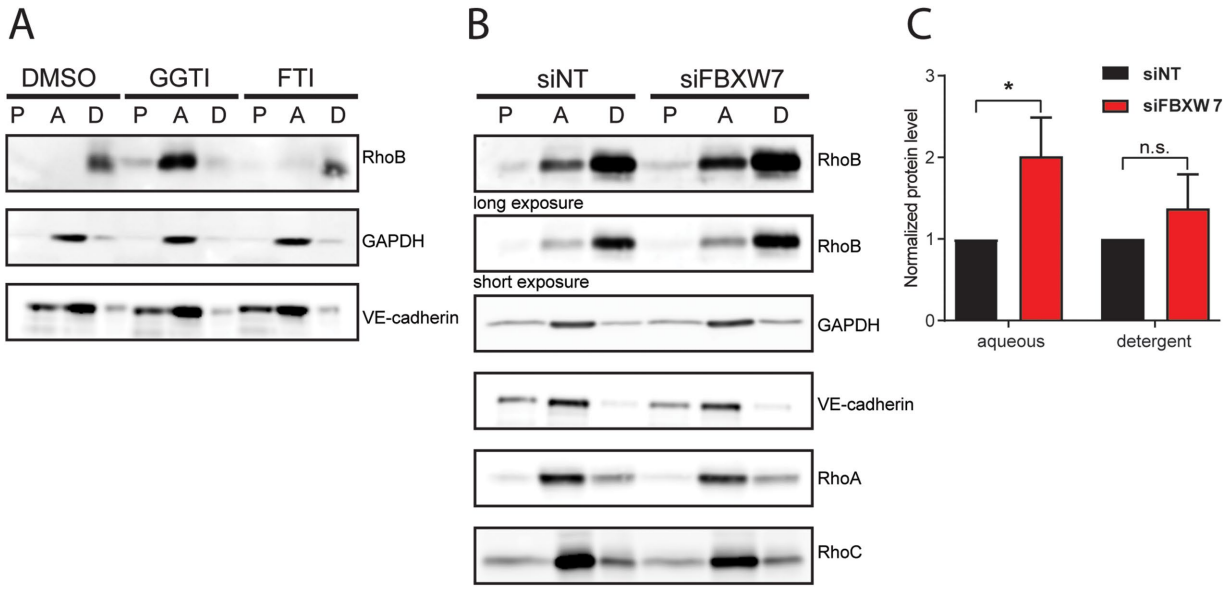

FIGURE 7: FBXW7 knockdown mimics impairment in RhoB prenylation induced by GGTI treatment. (A) Western blot showing RhoB expression in protein fractions obtained from HUVECs after Triton X-114 extraction followed by centrifugation on 6% sucrose cushion solution. The cells were pretreated with dimethyl sulfoxide, GGTI, or FTI for 18 h. P, Triton-insoluble pellet; A, aqueous fraction; and D, detergent-rich lipid droplet. GAPDH is shown as loading control. (B) Western blot of RhoA, RhoB, and RhoC in samples obtained as in A from HUVECs transfected with control or FBXW7 siRNA at 72 h posttransfection. (C) Quantification of RhoB immunoblot from B. Bar graph represents mean ± SD of RhoB expression in aqueous and detergent-rich fraction from three individual experiments, all relative to GAPDH and normalized to siNT. *, $p < 0.05$.

Penter *et al.*, 2015). However, our study is the first to analyze the function of F-box proteins in the regulation of the endothelial barrier. In vivo work by Izumi and colleagues showed that an endothelial-specific knockout of FBXW7 leads to increased activation of the Notch pathway, which results in decreased angiogenesis (Izumi *et al.*, 2012). In addition, Tsunematsu and coworkers reported that FBXW7 knockout mice are not viable due to impaired vascular development (Tsunematsu *et al.*, 2004). FBXW7 was also shown to be involved in regulation of angiogenesis, via ubiquitination of KLF2 in ECs (Zhao *et al.*, 2013). Together, these previous findings already indicate that FBXW7 is an important pleiotropic regulator of vascular dynamics.

We recently reported that knockdown of FBXW7 by shRNAs leads to increased stress fiber formation (Kovačević *et al.*, 2018). Also, we found that inhibition of ubiquitination greatly increased the level of RhoB in ECs. In this situation, RhoB localizes diffusely throughout the cells and at the plasma membrane (Kovačević *et al.*, 2018). In the current study, we show that RhoB protein is increased and mainly detected in vesicles upon loss of FBXW7. This suggests that, besides ubiquitination of RhoB, additional mechanisms might regulate RhoB localization upon depletion of FBXW7 in ECs.

Given the known function of FBXW7 in controlling SREBP ubiquitination (Sundqvist *et al.*, 2005; Loregger *et al.*, 2017), we tested whether the cholesterol synthesis pathway is affected in FBXW7 knockdown HUVECs (Loregger *et al.*, 2017). Indeed, we found an increase in the SREBP-2–regulated program in siFBXW7-transfected ECs. This is in good agreement with data from Sundqvist and coworkers, who showed that depletion of FBXW7 stabilized SREBP in the nuclei of HCT116 cells and increased expression of SREBP target genes like *LDLR* and *HMGCR* (Sundqvist *et al.*, 2005). The same effect was described by Onoyama and colleagues, who found that knockdown of FBXW7 leads to liver steatosis and hamartoma development, due to hepatic accumulation of lipids (Onoyama *et al.*, 2011).

FBXW7 regulates degradation of many target proteins (e.g., SREBP-1 and -2, Myc, Notch-1, and cyclin E), and this promiscuity of FBXW7 hinders clear dissection of the molecular mechanism behind the endothelial barrier disruption in FBXW7-depleted cells. Nevertheless, by using low-proliferating, close to confluent primary human ECs in low passages, we minimalized potential effects of FBXW7 loss on cell proliferation. Clear up-regulation of the cholesterol synthesis pathway, rescue of the phenotype by enhanced geranylation, and RhoB depletion all suggest that the impairment in the FBXW7-prenylated RhoB signaling axis plays a major role in disruption of endothelial barrier integrity upon FBXW7 depletion.

FTIs and GGTIs were previously used to study the effects of prenylation on expression and localization of RhoB. These studies have shown that FTI induces a shift toward geranylgeranylated RhoB, while GGTI leads to a shift toward farnesylated RhoB. As described previously, geranylgeranylated RhoB is localized in vesicles (Wherlock *et al.*, 2004; Von Zee and Stubbs, 2011). Immunofluorescence staining in this study revealed that RhoB is localized in vesicles in FBXW7 knockdown cells, which resembles localization of RhoB in control cells treated with FTI. This suggests that there is more geranylgeranylated RhoB in FBXW7 knockdown cells when compared with control cells. Interestingly, addition of FTI to FBXW7 cells slightly decreased the levels of RhoB, suggesting that there is also farnesylated RhoB in FBXW7 knockdown cells and that farnesylation might protect RhoB from degradation. In accordance with this, addition of GGTI to the control and FBXW7 knockdown cells caused an increase in RhoB protein levels and localization of RhoB outside vesicles. GGTI treatment also caused a redistribution of RhoB from the detergent-rich lipophilic cell lysate fraction to the aqueous hydrophilic fraction. This was to some degree similar in FBXW7

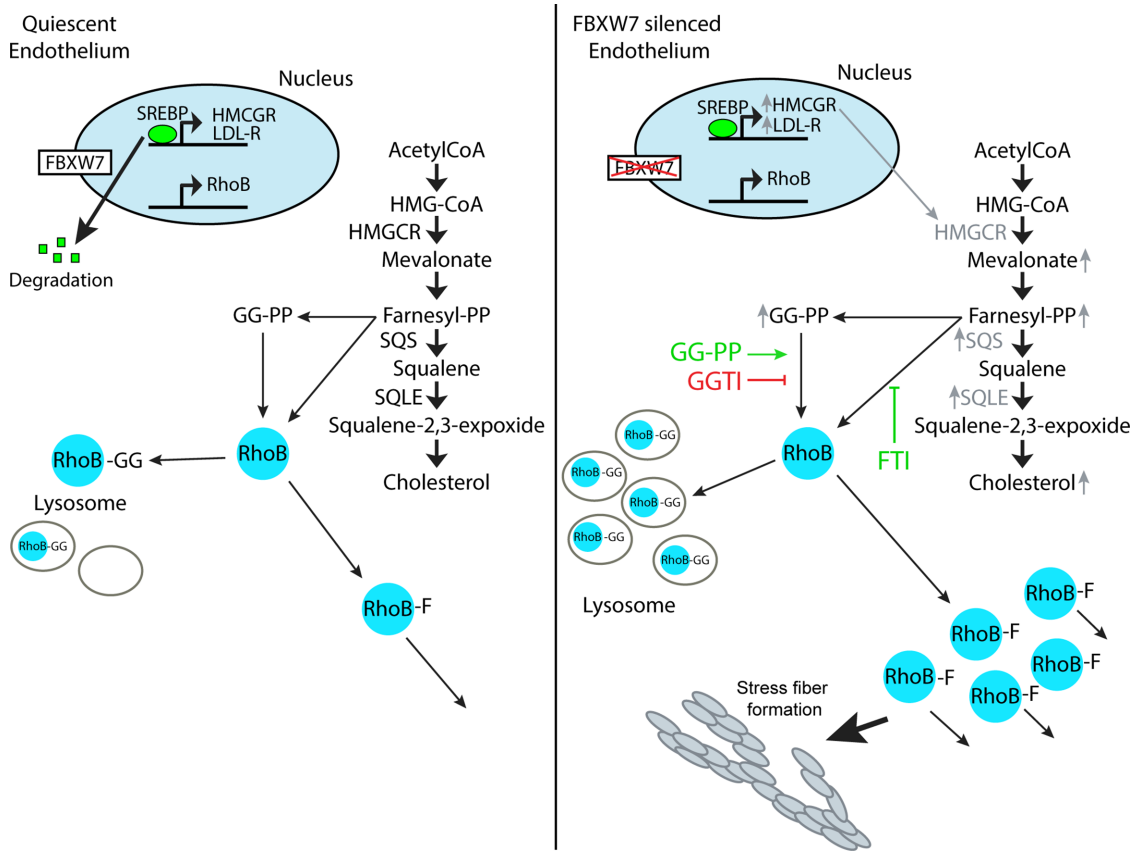

FIGURE 8: Proposed model of regulation of endothelial barrier function by FBXW7. In quiescent endothelium, SREBP is efficiently degraded via the proteasome because of FBXW7-mediated ubiquitination, so there is no or little activation of the cholesterol pathway. RhoB is expressed at low levels; the expressed RhoB is modified with a geranylgeranyl group to be inactive and stored in vesicles or with a farnesyl group to be active at the cell periphery. Upon loss of FBXW7, SREBP is stabilized, which results in activation of the cholesterol pathway by induction of HMCGR. Therefore, more GGPP and FPP is generated to modify RhoB. More RhoB will accumulate in the vesicles, but more RhoB will also be active at the cell periphery, inducing stress fiber formation and contraction. Addition of FTI will rescue this effect, because this induces geranylgeranylation of RhoB, an effect that is mimicked by GGPP. Addition of GGTI will lead to a switch toward farnesylation of RhoB that promotes its signaling at the plasma membrane and thus is detrimental for endothelial barrier function.

knockdown cells, where RhoB also increased in the aqueous hydrophilic fraction. These findings suggest that both farnesylation and geranylgeranylation of RhoB are impaired in FBXW7 knockdown cells.

Knockdown of FBXW7 and/or stimulation with FTI and GGTI resulted in differential effects on actin stress fiber formation. The increased stress fiber formation in FBXW7 knockdown cells is likely due to increased expression of RhoB, as RhoB promotes stress fiber formation (Pronk *et al.*, 2017). There is evidence that geranylgeranylated RhoB (Du *et al.*, 1999), as well as farnesylated RhoB, can induce stress fiber formation (Duluc *et al.*, 2017). Because FTI treatment or supplementation of cell medium with GGPP partially rescue the contractile phenotype and loss of endothelial integrity in FBXW7 knockdown cells, it is conceivable that the major form of RhoB, which induces contraction, is not the geranylgeranylated but the farnesylated one. FTI application promotes the switch toward the geranylgeranylated form of RhoB, which is translocated to intracellular vesicles for degradation. In contrast, addition of GGTI increases the farnesylated form of RhoB, which is less efficiently degraded and may induce contraction.

In conclusion, we found that perturbations in the FBXW7-regulated cholesterol synthesis pathway and, consequently, protein prenylation disrupt endothelial integrity. Altered prenylation of RhoB upon FBXW7 knockdown appears to be the main cause of this effect. This indicates that tight regulation of the expression and activity of RhoB levels is essential for the maintenance of endothelial integrity.

MATERIALS AND METHODS

Antibodies, reagents, and siRNAs

The following antibodies were used for immunostaining: α-VE-cadherin XP (#2500; Cell Signaling Technologies, Danvers, MA) and a-RhoB (#sc-8048; Santa Cruz Biotechnology, Santa Cruz, CA). Alexa Fluor 488 secondary antibody (anti-rabbit and anti-mouse) and Alexa Fluor 647 secondary antibody (anti-rabbit) (all Invitrogen) were the secondary antibodies.

The following antibodies were used for protein analysis: ß-actin (Merck), LDLR (Biovision), and SQLE (Proteintech). α-p44/42 MAPK (ERK1/2) (#9102), α-RhoA (#2117), α-RhoC (#3430), and α-GAPDH (#2118; Cell Signaling Technologies), α-RhoB (#sc-180, #sc-8048; Santa Cruz Biotechnology), α-HA (H3663), and α-vinculin (V4139; Sigma-Aldrich), α-Fbxw7 (ab171961; Abcam) and mouse α-ubiquitin (FK-2; Boston Biochem). HRP-conjugated goat–anti-rabbit antibody and goat–anti-mouse (Dako) were used as secondary antibodies.

For inhibition of geranylgeranylation and farnesylation, GGTI-298 and FTI-277 HCL (both Selleck Chemicals) were used. For normalization of prenylation in the FBXW7 knockdown cells, GGPP or FPP were applied (Sigma).

The siRNAs used were ON-TARGET plus Nontargeting pool (siNT), ON-TARGET plus Human FBXW7 pool (siFBXW7), ON-TARGET plus Human RHOA siRNA pool (siRhoA), ON-TARGET plus Human RHOB siRNA pool (siRhoB), and ON-TARGET plus Human FBXW7 siRNA—Set of 4 Upgrade (all Dharmacon/GE-Healthcare, Lafayette, CO).

Cell culture

Primary HUVECs were isolated from umbilical cords obtained from the department of obstetrics of the Amstelland Ziekenhuis (Amstelveen, The Netherlands). ECs were isolated and cultured as described previously (Jaffe *et al*., 1973). Informed consent was obtained from all donors in accordance with the institutional guidelines and the Declaration of Helsinki. After isolation, cells of three different donors were pooled and cultured on 1% gelatin-coated plate in M199 medium supplemented with 100 U/ml penicillin and 100 µg/ml streptomycin, 2 mmol/l L-glutamine, 10% heat-inactivated newborn calf serum (all Lonza, Verviers, Belgium), 10% heat-inactivated human serum (Invitrogen), 150 µg/ml crude endothelial growth factor (prepared from bovine brains), and 5 U/ml heparin (Leo Pharmaceutical Products, Breda, The Netherlands). Cells were cultured at 37°C and 5% CO_2 with the medium changed every other day. For all experiments, pools of three donors were used in passage 2 or 3.

HEK293T cells (American Type Culture Collection) were cultured in DMEM (Life Technologies) supplemented with 100 U/ml penicillin and 100 µg/ml streptomycin, 2 mM L-glutamine (all Lonza), 1 mM sodium pyruvate (Life Technologies), and 10% fetal bovine serum (PAA Laboratories).

esiRNA screen

A custom MISSION esiRNA library (Sigma-Aldrich) targeting 62 human F-box proteins was ordered on a 96-well microtiter plate (Table 1). EGFP and KIF11 esiRNAs were used as controls. Subconfluent p1 HUVECs were seeded on 1% gelatin–coated 96 W10idf ECIS arrays (Applied Biophysics, Troy, NY) in complete medium, 24 h before transfection. Forward transfection of esiRNAs with DharmaFECT 1 was performed according to the manufacturer's instructions using esiRNA at 100 ng final concentration and 0.2% (vol/vol) of DharmaFECT 1 transfection reagent (Dharmacon/GE-Healthcare) in 100 µl total volume. After 16 h, medium was replaced by normal culturing medium to avoid toxicity.

Transfection with siRNA

HUVECs were transfected with DharmaFECT 1, according to the manufacturer's protocol (Dharmacon/GE-Healthcare). Transfection was performed with a final concentration of 25 nM siRNA and 0.2% (vol/vol) DharmaFECT 1 in 10% NBCSi/M199 per condition. Transfection was done on cells that were ~80% confluent in 96-well, 12-well and six-well format. Medium was replaced after 16 h of transfection with regular cell culture medium to avoid toxicity.

Endothelial barrier function assays

Endothelial barrier function was measured with ECIS and passage of HRP. For ECIS measurements, cells were seeded at 1:1 density on gelatin-coated 96-well ECIS plates or eight-well arrays containing gold intercalated electrodes (Applied Biophysics). At 24 h after seeding, cells were transfected using DharmaFECT 1 and siRNAs for 16 h. At 72 h after transfection, cells were serum-starved with M199 supplemented with 1% human serum albumin (HSA; Sanquin CLP) for 90 min. Subsequently, a thrombin mix was added to the wells with a final concentration of 1 U/ml (Sigma-Aldrich). During the growth phase, resistance was measured at multiple frequencies to allow calculation for changes in cell–cell adhesion (Rb) and cell–matrix interaction (α).

For measurement of HRP passage, ECs were transfected in a six- or 12-well plate for 24 h before passaging 2:1–1% gelatin–coated 0.33 cm^2 polyester ThinCerts cell culture inserts (Greiner Bio-one) with a pore size of 3.0 µm. Approximately 72 h after the start of transfection, cells were serum-starved with 1% HSA/M199, which was added to the filters for 60 min. Before stimulation, medium in the upper compartment was replaced with 1% HSA/M199 containing 5 µg/ml HRP (Sigma-Aldrich) and 1 U/ml thrombin or a vehicle control; 1% HSA/M199 was added to the lower compartment. A sample was taken from the lower compartment at different time points. The HRP concentration was calculated by measuring absorption after adding tetramethylbenzidine (Upstate/Millipore) and sulfuric acid.

Triton X-114 protein extraction

This experiment was performed with some modifications according to Mohamed *et al*. (2018). In brief, confluent monolayers of primary HUVECs seeded on 10 cm^2 culture wells were lysed on ice in Triton X-114–containing lysis buffer (20 mM Tris-HCl, pH 7.5, 150 mM NaCl, 1% Triton X-114, and protease inhibitor cocktail [Roche]). Cells were scraped, and lysates were briefly centrifuged at 13,000 × *g*. Triton X-114–insoluble pellet (P) was dissolved in sample buffer. Supernatant was carefully loaded on 6% cushion solution (20 mM Tris-HCl, pH 7.4, 150 mM NaCl, 6% sucrose, 0.06% Triton X-114, and protease inhibitor cocktail) and incubated for 10 min at 37°C. After 5 min centrifugation at 16,000 × *g*, fractions were separated into aqueous (A) supernatant and detergent-rich lipid-containing droplet (D). All fractions were boiled with sample buffer and analyzed by immunoblotting. Before lysis, HUVECs were transfected with control or FBXW7 siRNA pools as described before or treated with GGTI or FTI for 24 h.

RhoB in vivo ubiquitination assay

HEK293T cells were cotransfected with mCherry-RhoB (Kovačević *et al*., 2018), hemagglutinin (HA)-ubiquitin (Kovačević *et al*., 2018), and FBXW7 plasmids (generous gift of C. Nicot, University of Kansas Medical Center) using Trans-IT-LT1 (#MIR 2300; Mirus) following the manufacturer's protocol. The next day, cells were treated with 2.5 µm MG132 for the last 4 h, and denaturing HA-immunoprecipitation was performed as described previously (Kovačević *et al*., 2018).

Lentiviral shRNA FBXW7 knockdown and overexpression

For the rescue experiment, we transduced ECs with shRNA targeting the 3′UTR of FBXW7 (TRCN0000355644; Sigma Mission Library, Sigma-Aldrich). Lentiviral particles were produced by transfecting HEK293T cells with the third generation HIV-1 packaging plasmids (Addgene), using Trans-IT-LT1 (Mirus) as previously described (Kovačević *et al*., 2018). For FBXW7 lentiviral overexpression, doxocycline-inducible pTripZ-FBXW7 (generous gift of C. Nicot, University of Kansas Medical Center) was packed into lentiviral particles using the same protocol. To induce the expression of FBXW7, 2 µg/ml doxocycline was added for 24 h to the cell medium.

Immunoprecipitation of RhoB

Immunoprecipitation of endogenous RhoB was performed with rabbit α-RhoB antibody (Santa Cruz Biotechnology) from confluent

60 cm^2 dishes of primary HUVECs transfected with control siRNA or FBXW7 siRNA. Proteasomal degradation was inhibited by adding 5 μM MG132 at 2 h before lysis. Upon stimulation, cells were washed in phosphate-buffered saline (PBS) containing 1 mM $CaCl_2$ and 0.5 mM $MgCl_2$ and lysed in lysis buffer (50 mM Tris, pH 7.4, 150 mM NaCl, 1 mM EDTA, 1% NP40, complete protease inhibitor cocktail tablets [Roche]) and phosphatase inhibitors (1 mM Na_3VO_4 and 25 mM NaF). Lysates were cleared by centrifugation and incubated with 1 μg RhoB antibody for 2 h at 4°C. RhoB-containing complexes were pulled out by incubation with Dynabeads protein G (Thermo scientific) for 1 h at 4°C. Finally, beads were washed four times with lysis buffer, and immunoprecipitated proteins were eluted with sample buffer and analyzed with SDS–PAGE.

Protein analysis

For analysis of protein levels, cells were seeded in 5 or 10 cm^2 culture wells and transfected as described earlier. At 72 h posttransfection, cells were washed with cold PBS and whole-cell lysates were collected by scraping the cells in the presence of 2X SDS sample buffer. Protein samples were loaded on 12.5% SDS–PAGE gels or NuPAGE Novex 4-12% Bis-Tris gels (Invitrogen), electrophoresed, and transferred to nitrocellulose membranes. Protein analysis was performed by incubation of the nitrocellulose membranes with the designated antibodies. Bands were visualized with enhanced chemiluminescence (Amersham/GE-Healthcare) on an AI600 machine (Amersham/GE-Healthcare).

Immunofluorescence imaging of cultured ECs

Transfected cells were seeded on 2 cm^2 and 12-mm glass coverslips (Menzel), coated with 1% gelatin and cross-linked with 0.5% glutaraldehyde (Sigma-Aldrich), ~24 h after the start of transfection. Cells were grown for 48 h with complete medium to reach the transfection time of 72 h. After cells were preincubated with 1% HSA/M199 for 1 h, thrombin was added to the wells in a final concentration of 1 U/ml. After 15 min or 3 h, cells were fixed with warm (37°C) 4% paraformaldehyde (PFA; Sigma-Aldrich) and put on ice for 15 min. The PFA was washed away with PBS, and cells were permeabilized with 0.2% Triton X-100 in PBS (Sigma-Aldrich) and blocked for 30 min with 1% bovine serum albumin (BSA). Then, coverslips were stained with primary antibodies against VE-cadherin or RhoB (in 0.1% BSA/PBS) for 1 h at room temperature. After being washed three times, the cells were incubated with a fluorescein isothiocyanate–labeled secondary antibody (anti-rabbit or anti-mouse 1:100 in 0.1% BSA/PBS) and Acti-stain phalloidin (direct staining, in 0.1% BSA/PBS [Tebu Bio]) at room temperature. After being washed, the cells were incubated with 4′,6-diamidino-2-phenylindole (DAPI; Thermo Fisher Scientific) at room temperature. Coverslips were mounted with Mowiol4-88/DABCO solution (Calbiochem, Sigma-Aldrich). Confocal-scanning laser microscopy was performed on a Nikon A2R confocal microscope (Nikon). Images were analyzed and equally adjusted with ImageJ.

RNA isolation and quantitative PCR

Isolation of total RNA and subsequent real-time quantitative PCR were done as previously reported (Loregger *et al.*, 2015). Sequences of quantitative PCR primers are available on request.

Statistical analysis

For the esiRNA screen, the observed values ($n = 4$) were compared with the EGFP controls by a Student's *t* test, after which the *p* values were corrected for multiple testing by using a Benjamini-Hochberg FDR set to <0.05.

For the other experiments, data are represented as mean ± SEM unless indicated otherwise. Comparison of two conditions was tested by Student's *t* test. Comparison of more than two conditions was tested by one-way analysis of variance (ANOVA) or repeated-measures ANOVA with Dunnett's post hoc test. The *p* values were considered statistically significant if $p < 0.05$. Analysis was performed using GraphPad Prism software.

ACKNOWLEDGMENTS

I.K. was supported by a grant (#1311) from the Landsteiner Foundation for Blood Transfusion Research (LSBR). M.C.A.P. was funded by the Rembrandt Institute for Cardiovascular Science. N.Z. is an established investigator of the Dutch Heart Foundation (2013T111) and is supported by an ERC Consolidator grant (617376) from the European Research Council and by a Vici grant from the Netherlands Organization for Scientific Research (NWO; 016.176.643). A.L. is supported by a Dekker grant from the Dutch Heart Foundation (2016T015). This work was supported by an Amsterdam Cardiovascular Sciences (ACS) "out of the box grant" to N.Z. and P.L.H.

REFERENCES

Abu Taha A, Schnittler H-J (2014). Dynamics between actin and the VE-cadherin/catenin complex. Cell Adh Migr 8, 125–135.

Adamson P, Marshall CJ, Hall A, Tilbrook PA (1992). Post-translational modifications of p21Rho proteins. Biol Chem 267, 20033–20038.

Ardley HC, Robinson PA (2005). E3 ubiquitin ligases. Biochemistry 41, 15–30.

Bolte S, Cordelieres FP (2006). A guided tour into subcellular colocalization analysis in light microscopy. J Microsc 224, 213–232.

Bos JL, Rehmann H, Wittinghofer A (2007). GEFs and GAPs: critical elements in the control of small G proteins. Cell 129, 865–877.

Cardozo T, Pagano M (2004). The SCF ubiquitin ligase: insights into a molecular machine. Nat Rev Mol Cell Biol 5, 739–751.

Cherfils J, Zeghouf M (2013). Regulation of small GTPases by GEFs, GAPs, and GDIs. Physiol Rev 93, 269–309.

Dejana E (1996). Endothelial adherens junctions: implications in the control of vascular permeability and angiogenesis. J Clin Invest 98, 1949–1953.

Du W, Lebowitz PF, Prendergast GC (1999). Cell growth inhibition by farnesyltransferase inhibitors is mediated by gain of geranylgeranylated RhoB. Mol Cell Biol 19, 1831–1840.

Duluc L, Ahmetaj-Shala B, Mitchell J, Abdul-Salam VB, Mahomed AS, Aldabbous L, Oliver E, Iannone L, Dubois OD, Storck EM, *et al.* (2017). Tipifarnib prevents development of hypoxia-induced pulmonary hypertension. Cardiovasc Res 113, 276–287.

Garcia-Mata R, Boulter E, Burridge K (2011). "The invisible hand": regulation of RHO GTPases by RHOGDIs. Nat Rev Mol Cell Biol 12, 493–504.

Giannotta M, Trani M, Dejana E (2013). VE-cadherin and endothelial adherens junctions: active guardians of vascular integrity. Dev Cell 26, 441–454.

Hodge RG, Ridley AJ (2016). Regulating Rho GTPases and their regulators. Nat Rev Mol Cell Biol 17, 496–510.

Hordijk PL, Anthony FP, Mul E, Rientsma LC, Oomen D, Roos D (1999). Vascular-endothelial-cadherin modulates endothelial monolayer permeability. J Cell Sci 112, 1915–1923.

Izumi N, Helker C, Ehling M, Behrens A, Herzog W, Adams RH (2012). Fbxw7 controls angiogenesis by regulating endothelial Notch activity. PLoS One 7, e41116.

Jaffe EA, Nachman RL, Becker CG, Minick CR (1973). Culture of human endothelial cells derived from umbilical veins. J Clin Invest 52, 2745–2756.

Kainulainen M, Lau S, Samuel CE, Hornung V, Weber F (2016). NSs virulence factor of Rift Valley fever virus engages the F-box proteins FBXW11 and beta-TRCP1 to degrade the antiviral protein kinase PKR. J Virol 90, 6140–6147.

Kovačević I, Sakaue T, Majoleé J, Pronk MC, Maekawa M, Geerts D, Fernandez-Borja M, Higashiyama S, Hordijk PL (2018). The Cullin-3–Rbx1 KCTD10 complex controls endothelial barrier function via K63 ubiquitination of RhoB. J Cell Biol 217, 1015–1032.

Lee WL, Slutsky AS (2010). Sepsis and endothelial permeability. N Engl J Med 363, 689–691.

Li H, Wang Z, Zhang W, Qian K, Xu W, Zhang S (2016). Fbxw7 regulates tumor apoptosis, growth arrest and the epithelial-to-mesenchymal transition in part through the RhoA signaling pathway in gastric cancer. Cancer Lett 370, 39–55.

Loregger A, Cook EC, Nelson JK, Moeton M, Sharpe LJ, Engberg S, Karimova M, Lambert G, Brown AJ, Zelcer N (2015). A MARCH6 and IDOL E3 ubiquitin ligase circuit uncouples cholesterol synthesis from lipoprotein uptake in hepatocytes. Mol Cell Biol 36, 285–294.

Loregger A, Raaben M, Tan J, Scheij S, Moeton M, van den Berg M, Gelberg Etel H, Stickel E, Roitelman J, Brummelkamp T, Zelcer N (2017). Haploid mammalian genetic screen identifies UBXD8 as a key determinant of HMGCR degradation and cholesterol biosynthesis. Arterioscler Thromb Vasc Biol 37, 2064–2074.

Machida YJ, Dutta A (2007). The APC/C inhibitor, Emi1, is essential for prevention of rereplication. Genes Dev 21, 184–194.

Mazieres J, Tillement V, Allal C, Clanet C, Bobin L, Chen Z, Sebti SM, Favre G, Pradines A (2005). Geranylgeranylated, but not farnesylated, RhoB suppresses Ras transformation of NIH-3T3 cells. Exp Cell Res 304, 354–364.

Mohamed A, Viveiros A, Williams K, Posse de Chaves E (2018). Aβ inhibits SREBP-2 activation through Akt inhibition. J Lipid Res 59, 1–13.

Moy AB, Winter M, Kamath A, Blackwell K, Reyes G, Giaever I, Keese C, Shasby DM (2000). Histamine alters endothelial barrier function at cell-cell and cell-matrix sites. Am J Physiol Lung Cell Mol Physiol 278, L888–L898.

Onoyama I, Suzuki A, Matsumoto A, Tomita K, Katagiri H, Oike Y, Nakayama K, Nakayama KI (2011). Fbxw7 regulates lipid metabolism and cell fate decisions in the mouse liver. J Clin Invest 121, 342–354.

Penter L, Maier B, Frede U, Hackner B, Carell T, Hagemeier C, Truss M (2015). A rapid screening system evaluates novel inhibitors of DNA methylation and suggests F-box proteins as potential therapeutic targets for high-risk neuroblastoma. Target Oncol 10, 523–533.

Pickart CM, Eddins MJ (2004). Ubiquitin: structures, functions, mechanisms. Biochim Biophys Acta 1695, 55–72.

Pronk MCA, van Bezu JSM, van Nieuw Amerongen GP, van Hinsbergh VWM, Hordijk PL (2017). RhoA, RhoB and RhoC differentially regulate endothelial barrier function. Small GTPases 1–19.

Schaefer A, Reinhard NR, Hordijk PL (2014). Toward understanding RhoGTPase specificity: structure, function and local activation. Small GTPases 5, 6.

Stamatakis K, Cernuda-Morollon E, Hernandez-Perera O, Perez-Sala D (2002). Isoprenylation of RhoB is necessary for its degradation. A novel determinant in the complex regulation of RhoB expression by the mevalonate pathway. J Biol Chem 277, 49389–49396.

Sundqvist A, Bengoechea-Alonso MT, Ye X, Lukiyanchuk V, Jin J, Harper JW, Ericsson J (2005). Control of lipid metabolism by phosphorylation-dependent degradation of the SREBP family of transcription factors by SCF(Fbw7). Cell Metab 1, 379–391.

Tsunematsu R, Nakayama K, Oike Y, Nishiyama M, Ishida N, Hatakeyama S, Bessho Y, Kageyama R, Suda T, Nakayama KI (2004). Mouse Fbw7/Sel-10/Cdc4 is required for notch degradation during vascular development. J Biol Chem 279, 9417–9423.

Van Nieuw Amerongen GP, Van Delft S, Vermeer MA, Collard JG, Van Hinsbergh VW (2000). Activation of RhoA by thrombin in endothelial hyperpermeability—role of Rho kinase and protein tyrosine kinases. Circ Res 87, 335–340.

Von Zee CL, Stubbs EB Jr (2011). Geranylgeranylation facilitates proteasomal degradation of rho G-proteins in human trabecular meshwork cells. Invest Ophthalmol Vis Sci 52, 1676–1683.

Wang Z, Liu P, Inuzuka H, Wei W (2014). Roles of F-box proteins in cancer. Nat Rev Cancer 14, 233–247.

Wei J, Mialki RK, Dong S, Khoo A, Mallampalli RK, Zhao Y, Zhao J. (2013). A new mechanism of RhoA ubiquitination and degradation: roles of SCF(FBXL19) E3 ligase and Erk2. Biochim Biophys Acta 1833, 2757–2764.

Wherlock M, Gampel A, Futter CE, Mellor H (2004). Farnesyltransferase inhibitors disrupt EGF receptor traffic through modulation of the RhoB GTPase. J Cell Sci 117, 3221–3231.

Wojciak-Stothard B, Ridley AJ (2002). Rho GTPases and the regulation of endothelial permeability. Vascul Pharmacol 39, 187–199.

Zhao S, Gou LT, Zhang M, Zu LD, Hua MM, Hua Y, Shi HJ, Li Y, Li J, Li D, *et al*. (2013). piRNA-triggered MIWI ubiquitination and removal by APC/C in late spermatogenesis. Dev Cell 24, 13–25.

Zhou ZD, Sathiyamoorthy S, Angeles DC, Tan EK (2016). Linking F-box protein 7 and parkin to neuronal degeneration in Parkinson's disease (PD). Mol Brain 9, 41.